Arabian Journal of Chemistry (2023) **16**, 104400

King Saud University

Arabian Journal of Chemistry

www.ksu.edu.sa
www.sciencedirect.com

ORIGINAL ARTICLE

Surface modification of pyrophyllite for optimizing properties of castor oil-based polyurethane composite and its application in controlled-release fertilizer

Shiping Wang [a], Xiang Li [a], Kun Ren [a], Rui Huang [a], Ganchang Lei [a], Lijuan Shen [b], Yingying Zhan [a,*], Lilong Jiang [a,*]

[a] *National Engineering Research Center of Chemical Fertilizer Catalyst, Fuzhou University, Fuzhou 350002, China*
[b] *College of Environmental Science and Engineering, Fujian Normal University, Fuzhou 350007, China*

Received 4 August 2022; accepted 5 November 2022
Available online 11 November 2022

KEYWORDS

Pyrophyllite;
Mechanochemical modification;
Controlled-release fertilizer;
Composite material;
Hydrolytic stability

Abstract The high cost and difficulty in sustainability have hindered the wide application of the general synthetic resins in the controlled-release fertilizers (CRF). Here, the degradable castor oil-based polyurethane (PU) was filled by the natural pyrophyllite (PY) powders, which were pre-modified with few amount (≤0.5 %) of NDZ-201 coupling agent though a simple and economic mechanochemical method. Furthermore, the composite materials of PU and the modified PY (MPY/PU) with enhanced comprehensive properties were prepared and applied in CRF. Moreover, the release behaviors of the coated fertilizers were investigated while tuning the addition amount of modifier or the filling amount of MPY, and it was confirmed that the release performance was highly depended on the hydrophobic and mechanical properties of the composite coating. As a result, the best optimized MPY/PU coating exhibited significantly superior performance to the pure PU materials, and the duration of 80 % nitrogen release was more than 40 days. This confirms that the MPY/PU composite is a promising coating material for the CRF granules.

* Corresponding authors.
E-mail addresses: wangsp@fzu.edu.cn (S. Wang), lixiang9597@163.com (X. Li), renkun601@163.com (K. Ren), huangrui308@163.com (R. Huang), lgc@fzu.edu.cn (G. Lei), ljshen@fjnu.edu.cn (L. Shen), zhanyingying@fzu.edu.cn (Y. Zhan), jll@fzu.edu.cn (L. Jiang).

Peer review under responsibility of King Saud University.

ELSEVIER Production and hosting by Elsevier

1. Introduction

Fertilizer is one of the important factors that limit the production of agriculture, and it has drawn intensive attentions to improve the efficiency of their use and minimize the possible adverse environmental impacts, particularly of nitrogenous fertilizers (Crews and Peoples, 2004). This can be done through the development of diverse slow or controlled-release fertilizers, including the matrix-formulations, the low-soluble organic-N compounds and the coated fertilizers (Kenawy et al., 2019; Kiran et al., 2019; Pereira et al., 2015;

https://doi.org/10.1016/j.arabjc.2022.104400
1878-5352

Sempeho et al., 2014; Vejan et al., 2021). The third type is constituted with a core–shell structure, that is, a fertilizer core is encapsulated by the inert materials, which play as the barriers to control the diffusion and release of the water-soluble fertilizers (Azeem et al., 2014). In this case, these coating materials with relatively low hydrophilicity, superior hydrolytic stability and good mechanical properties are highly in demand to resist the fast release of fertilizers. Besides, the cost and sustainability of the applied materials are also important factors that are considered by researchers (Beig et al., 2020; Fertahi et al., 2021; Tian et al., 2019; Wang et al., 2016).

Currently, diverse inorganic and synthetic organic materials have been developed as the coating materials (Lawrencia et al., 2021). Although the inorganic materials, such as sulfur (Haseeb ur et al., 2022; Snyder and Gasch, 1976; Zheng et al., 2016), gypsum and silicates (Dubey and Mailapalli, 2019; Eghbali Babadi et al., 2015; Eghbali Babadi et al., 2021; Souza et al., 2018), are well accessible and cheap, their controlled-release property are usually disappointing due to poor mechanical properties. Conversely, the synthetic organic materials, including polystyrene (Yang et al., 2012), polyether sulfone and polyurethane (Bortoletto-Santos et al., 2020; Emami et al., 2017; Liu et al., 2019; Wang et al., 2019), commonly have better controlled-release performance, but being disadvantaged for the high cost and poor degradability. While filling the inorganic materials into the synthetic organic ones (Chen et al., 2021; Hu et al., 2016; Li et al., 2018; Li et al., 2016; Salimi et al., 2020), the composite materials with reduced cost often perform comprehensive performance. Therefore, the inorganic/organic composite materials, especially the natural biomass-derived ones (Alisani et al., 2022; Das and Ghosh, 2022; Fertahi et al., 2021; Hu et al., 2021; Lohmousavi et al., 2020), are highly attractive.

Alternatively, the pyrophyllite ($Al_2[Si_4O_{10}](OH)_2$) is a natural clay mineral with a sheet-like structure, which has been widely applied in industries because of their unique properties, such as chemically inert and electrically neutral that makes it highly resistant to the strong acids and alkalis (Ali et al., 2021; Harvey and Murray, 1997; Qin et al., 2020). Specially, as a filler in the paint and plastic industry, the pyrophyllite can increase the resistance to film cracking and promote good dispersion due to the platy configuration originated from the silicate structure of the pyrophyllite sheets (Ali et al., 2021; Haitao et al., 2012). In addition, the high oil-absorption property of pyrophyllite is advantageous for excellent mixture between pyrophyllite and oleo-resinous materials (Pradhan et al., 2015). Commonly, the particles size and the surface property of the pyrophyllite need to control for the uniform dispersion of their powders within the matrix, which is depended on the industry in question. For instance, finely ground pyrophyllite is used in paints as a pigment extender and suspending agent (Canada, 2014; Erdemoğlu et al., 2004). On the other hand, low cost, low volatility and low toxicity of the modifiers were also important for the surface modification. Although the pyrophyllite has been widely used as inorganic fillers in various materials, its application in the field of controlled-release fertilizers is still lack of research.

Herein, the pyrophyllite powders (PY) were employed as the fillers in the degradable castor oil-based polyurethane (PU), which was further coated on the urea granules to produce controlled-release fertilizers (CRF). To optimize the chemical and structural properties of the pyrophyllite powders and their composites with the polyurethane matrix, the pyrophyllite powders were mechanochemically pretreated with various amounts ($\leq$0.5 wt%) of titanate coupling agent (NDZ-201) with low toxicity and low volatility. By this method, the dispersibility of the PY in the polyurethane matrix and their compatibility were adjusted, and the comprehensive properties of the composite materials were correspondingly optimized, including water swelling, hydrolytic stability, hydrophobic and mechanical properties. Specially, the controlled-release properties of the related PY/PU composites were investigated while coating on the urea fertilizer granules. In addition, the effect of the filling amount of the modified PY on these properties of the composite materials was also studied under a certain dosage of coupling agent.

2. Experimental section

2.1. Materials

Pyrophyllite ($Al_2[Si_4O_{10}](OH)_2$, PY), titanate coupling agent (NDZ-201), castor oil and urea granules (less than5 mm) are industrial grade reagents and used after fully drying. The castor oil had a hydroxyl number ($OH_{\#}$) of 163.0 mgKOH/g and a saponification number of 176.0–187.0 mgKOH/g. Toluene diisocyanate (TDI) and p-diamino benzaldehyde are analytical grade and purchased from Aladdin Reagent (Shanghai) Co., ltd. Other reagents are analytical grade and purchased from Sinopharm Chemical Reagent Co., ltd.

2.2. Preparation of the modified pyrophyllite (MPY)

First, the emulsion solution of NDZ-201 was prepared by stirring the mixture of titanate coupling agent and isopropanol with a mass ratio of 1 in a beaker. Then, 10.0 g pyrophyllite and various amount of the prepared NDZ-201 emulsion solution were added into a cup of ball mill, which contained 60 g agate balls, and the mass ratio of large balls, medium balls and small balls was 1:3:6. After that, the modified pyrophyllite powders were prepared by ball milling at a high speed of 500 r/min for 45 min, and the products were recorded as xMPY, where $\times$ was the addition amount of NDZ-201 relative to the PY.

2.3. Preparation of the pyrophyllite/polyurethane (MPY/PU) composite

The preparation of the degradable castor oil-based polyurethane and its composites were based on previous reports (Ristić et al., 2012; Yeganeh and Mehdizadeh, 2004). Typically, the castor oil (CO) and toluene diisocyanate (TDI) were firstly mixed in a round bottom flask with the equal molar amounts of hydroxyl and isocyanate groups. Then, various amount of MPY powders were added into the mixture solution, which was ultrasonically treated without heating for 20 min, so that the MPY powders can evenly disperse in the precursor solution. Later, this precursor solution was placed in a vacuum drying oven to remove any possible bubbles. Finally, the precursor solution was poured into a mold and cured at 45 °C for 24 h to prepare the MPY/PU composite films, which were denoted as xMPY/PU-y, where y was the filling amount of MPY in the polyurethane matrix and $\times$ was the same as mentioned above. The detail information of different samples was presented in the Table S1 of the supporting information.

2.4. Preparation of the coated CRF granules

The coated CRF granules were prepared with the urea granules as cores and the MPY/PU composites as the outer membrane. The urea granules in a size around 4 mm were firstly placed into a drum coating machine with a rotating speed of 40 rpm, meanwhile preheating the urea granules to reach a surface temperature in the range of 65 to 70 °C. After that, the above precursor solution was sprayed onto the surface of the urea granules with a spray gun, and then following a cure pro-

cess. By repeating these processes for several times, the coated CRF granules with a mass percentage of the coating membrane about 3 wt% were obtained, and the products were labeled as xMPY/PCU-y, where × and y were the same as mentioned above, and the PCU represented the polyurethane coating urea.

2.5. Characterizations

Fourier transform infrared spectrometer (FT-IR) (Nicolet 6700, Thermo Fisher Scientific Co., USA) was used to record the FT-IR spectra of series samples. The X-ray powder diffraction (XRD) patterns for different samples were recorded on an X-ray powder diffractometer (X'pert Pro, Panalytical, Netherlands) with Cu Kα radiation (1.542 nm). The surface composition and chemical structure of the modified pyrophyllites were analyzed by the X-ray photoelectron spectrometer (XPS, ESCALAB 250, Thermo Scientific Co., USA). The N_2 physisorption data of the modified pyrophyllites were obtained from a N_2 physical adsorption apparatus (ASAP 2020, Mircomeritics, USA), and the powders were degassed at 200 °C for 3 h. In addition, the physical structure of the PY, MPY and the membrane on the urea granules were observed by a Field-Emission Scanning Electron Microscope (S-4800, Hitachi, Japan).

2.6. Evaluation of hydrophobic property

The surface hydrophobic property of the modified pyrophyllites (MPY) and their composites with polyurethane was analyzed by recording the water contact angels on a contact angle measuring instrument (OCA25, Dataphysics, Germany). Before the measurement, the MPY powders were pressed into a uniform sheet at 40 kPa, and the water contact angels of the MPY/PU composites were tested with the films prepared as mentioned above.

2.7. Evaluation of water swelling property

To further analyze the water swelling property of the MPY/PU composite films, they were immersed into 200 mL deionized water. After holding at 25 °C for 24 h, the films were moved out and wiped off excess water on the surface with cotton papers before weighing. The formula for the calculating of water absorbency was as follows:

$$\text{Water Absorbency}\,(\%) = \frac{W_t - W_i}{W_i} \times 100\%$$

In the formula, W_i (g) was the mass of the composite materials before water-swelling. W_t (g) was the mass of the composite materials after water swelling.

2.8. Evaluation of mechanical property

The uniaxial tensible testing of the pyrophyllite/polyurethane composites was implemented on an electronic universal testing machine (C25.101, XinSanSi Enterprise Development Co., ltd, Shanghai) at a crosshead speed of 5 mm/min under room temperature. Before measurement, the dumbbell-shaped specimens of 4 mm width, 75 mm length and 0.8 mm thickness were prepared by pouring the degassed precursor solution into the mold and curing at 45 °C for 24 h.

2.9. Evaluation of hydrolytic stability

To analyze the hydrolytic stability of the pyrophyllite/polyurethane composite materials, a series of the dumbbell-shaped specimens were immersed into 200 mL deionized water, and sealed to heat at 60 °C for 7 days. After that, the specimens were moved out and the excess water was wiped off with cotton papers. According to the same testing method as above, the mechanical properties of these pre-treated specimens were evaluated, and the retention efficiency of the tensible strength was calculated while comparing to the original one.

2.10. Evaluation of the controlled-release behavior

The coated CRF granules about 5.0 g were firstly placed into nylon filter bags, which were further immersed into 100 mL deionized water at 25 °C. At the fixed intervals, the solutions were taken out, and the granules were rinsed fully before 100 mL new deionized water was added. The concentration of the released nitrogen (N) in the solutions were evaluated by a UV/Vis spectrophotometer (Lambda 950, Perkin Elmer, USA). To perform this measurement, the p-diamino benzaldehyde dissolved in the mixture solution of absolute ethanol and concentrated hydrochloric acid was employed as the color developer, and the absorbance was recorded at the wavelength of 430 nm. Finally, the N release was analyzed with a timely-used standard curve, and the cumulative release percentage of N at an incubation time of t was calculated as follows:

$$\text{Nitrogen release}\,(\%) = \frac{W_t}{W_T} \times 100\%$$

In the formula, W_t (mg) was the nitrogen release amount at an incubation time of t, and W_T (mg) was the total nitrogen content in the original coated CRF granules.

3. Results and discussion

3.1. Chemical and structural properties of the MPY

In this study, a natural clay of layered pyrophyllite (PY) was modified with few amounts (≤0.5 %) of titanate coupling agent (NDZ-201) via a facile, green and economic mechanical chemical approach. The modified PY (MPY) was further employed as a reinforced filler for the castor oil-based polyurethane (PU), which was spray-coated on the urea granules to produce controlled-release fertilizer. The preparation processes were proposed and illustrated as shown in Scheme 1.

The chemical structures of the PY and the related MPY samples modified with 4 wt% NDZ-201 were investigated by the FT-IR spectra (Fig. 1). The characteristic sharp peaks at 3674 cm^{-1} (ν_s, Al-OH) and 949 cm^{-1} (ν_δ, Al-OH) were presented in the FT-IR spectrum of the pyrophyllite (Fig. 1 A). The broad peak around 3423 cm^{-1} was due to the stretching vibration of OH from water and Si-OH. In addition, the peaks at 1120 cm^{-1}, 1069 cm^{-1} and 1051 cm^{-1} were attributed to the stretching vibration of Si-O bonds (Zhao et al., 2003). The clearly observed doublet peaks at 772 and 796 cm^{-1} and the

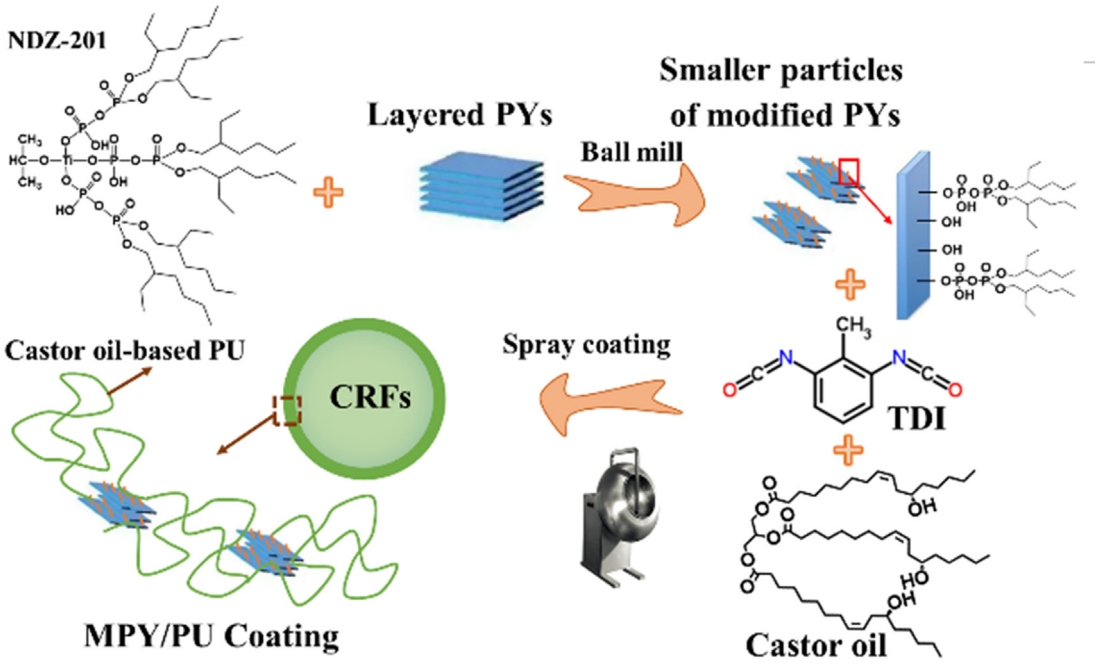

Scheme 1 Schematic illustration of the preparation processes for the MPY/PU coated urea granules.

one at 694 cm^{-1} were owing to the stretching vibration of Si-O-Si from the SiO_4 tetrahedron in the presence of quartz (Temuujin et al., 2003; Yu et al., 2010). Besides, the peak around 650–460 cm^{-1} were mainly originated from the bending vibration of Si-O-Si bonds (Monash and Pugazhenthi, 2010). For the FT-IR spectrum of NDZ-201, the characteristic peaks included the one at 2964 cm^{-1} for the $–CH_3$ asymmetrical stretching vibration, the one at 2931 cm^{-1} for the $–CH_2$- asymmetrical stretching vibration, and the wide overlapped one around 2866 cm^{-1} for the symmetrical stretching vibration of $–CH_3$ and $–CH_2$- (Liu et al., 2013). Correspondingly, their bending vibrations resulted in the peaks at 1462 and 1379 cm^{-1}. In addition, the peaks in the range of 1250–950 cm^{-1} were attributed to the stretching vibration of P—O, and the bending vibration of O—P—O bridge was occurred around 504 cm^{-1} (Boonchom and Baitahe, 2009; Parekh and Joshi, 2007).

After mechanochemically treated with NDZ-201, the MPY sample still held these characteristic peaks of Al-OH and Si-O-Si as confirmed by the FT-IR spectra in the Fig. 1 A. However, the peak at 3674 cm^{-1} (ν_s, Al-OH) for the MPY sample was weaker than the related one for the original PY, indicating that some of the surface Al-OH groups were reacted with the NDZ-201. Meanwhile, the broad peak around 3423 cm^{-1}became more obvious in the FT-IR spectra of MPY, which should be due to the dehydration of the Ti-OH groups formed during the surface modification (Song et al., 2019). Besides, three peaks at 2958 cm^{-1}, 2923 cm^{-1} and 2853 cm^{-1} were presented by the MPY sample (Fig. 1 B), which were owing to the C—H stretching vibration of the alkane groups. However, the wavenumbers of these peaks were different from the ones (2964, 2931 and 2866 cm^{-1}) in the FT-IR spectrum of NDZ-201, and the adsorptions for the asymmetrical and symmetrical stretching of $–CH_3$ were clearly decreased. These phenomena were possibly due to the hydrolysis of the alkoxy groups (Ti-O-CH$(CH_3)_2$) and the escape of isopropyl alcohol ($(CH_3)_2CHOH$).

The XPS spectra of the xMPY samples modified with various amount of NDZ-201 were further measured as shown in Fig. 1 C-F. The Al 2p XPS spectrum of the un-modified PY was located at 75.2 eV (Fig. 1 C), which was increased by 0.2 eV for the xMPY samples. Furthermore, the peak for Si 2p was also shifted to a higher binding energy after modifying the PY with different amount of NDZ-201 (Fig. 1 D). These results were due to the formation of Al—O—P and Si—O—P bonds during the surface modification. Meanwhile, compared to the Ti 2p XPS spectrum of NDZ-201 (Fig. 1 E), the peak for the 0.5MPY sample was shifted to a lower binding energy, possibly due to the formation of Ti-OH bonds. Furthermore, the P 2p XPS spectrum of the NDZ-201 presented a peak at 133.6 eV (Fig. 1 F), assigning to the $-PO_3(OH)$ and $-OPO_3$-structures of the NDZ-201 (Figure S1) (Amaral et al., 2012), which was changed to a higher binding energy around 134.8 eV for the MPY samples (Fukushima et al., 2016). These results were in accordance with the transformation of Ti—O—P to Al—O—P and Si—O—P bonds, further confirming the results of the FT-IR measurements. In addition, the TG curves of PY and 0.4MPY (Figure S2) were respectively showed a mass loss of 3.70 % and 4.05 % after heating to 1000 °C, revealing a difference of 0.35 %. This value was closed to the percentage of NDZ-201 added in the original PY during preparation process, indicating a high utilization efficiency of the coupling agent.

Besides, the physical structures of the PY and MPY samples were also investigated. As shown in the SEM images (Fig. 2 A, B), the original PY powders were irregular morphology of particles with layered structures. After the ball milling treatment, the size of the PY particles were obviously reduced (Fig. 2 C, D and Figure S3), and the layered structures were partially destroyed to form some fine flake-like structures. This was because that the layered peeling can happen along the interlayer face of the PY particles under strong mechanical force, and the fracture meanwhile occurred to facilitate the for-

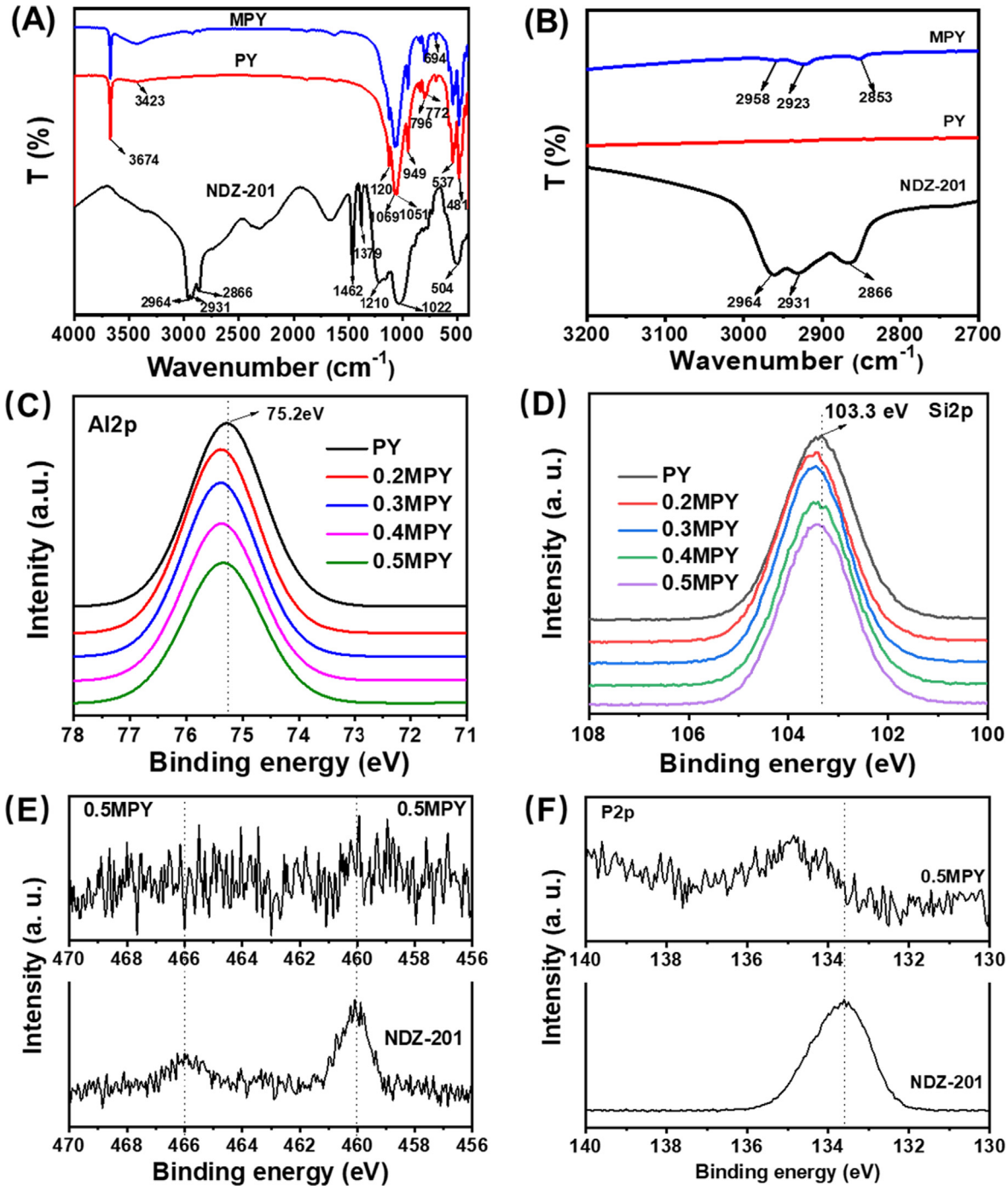

Fig. 1 (A) FT-IR spectra of NDZ-201, pyrophyllite and the MPY sample modified with 0.4 % NDZ-201. (B) The magnified spectra in the wavenumber range of 2800 to 3000 cm^{-1}. The XPS spectra of the NDZ-201, PY and the related modified PY with different addition percentage of coupling agent: (C) Al2p XPS spectra, (D) Si2p XPS spectra, (E) Ti2p XPS spectra and (F) P2p XPS spectra.

mation of refined particles (Chen et al., 2012; Lin and Zhao, 2019). Correspondingly, the specific surface area of the PY powders was 5.98 m^2 g^{-1}, which increased to 20.28 m^2 g^{-1} for the ball-milled PY without the coupling agent (Table 1). Specially, the PY particles were further refined after adding NDZ-201 in the ball milling system (Fig. 2 E, F), and the specific surface area of the xMPY samples were increased as the increased amount of NDZ-201. This indicated the synergistic effects of the coupling agent and the mechanical force on the exfoliation of PY particles. However, the specific surface area of the xMPY samples were decreased when the addition amount of NDZ-201 beyond 0.4 wt%, possibly due to the lubrication effect of the excess coupling agent, which can reduce the frictional force of the PY particles during ball milling and result in the production of larger PY particles (Figure S3 g, h).

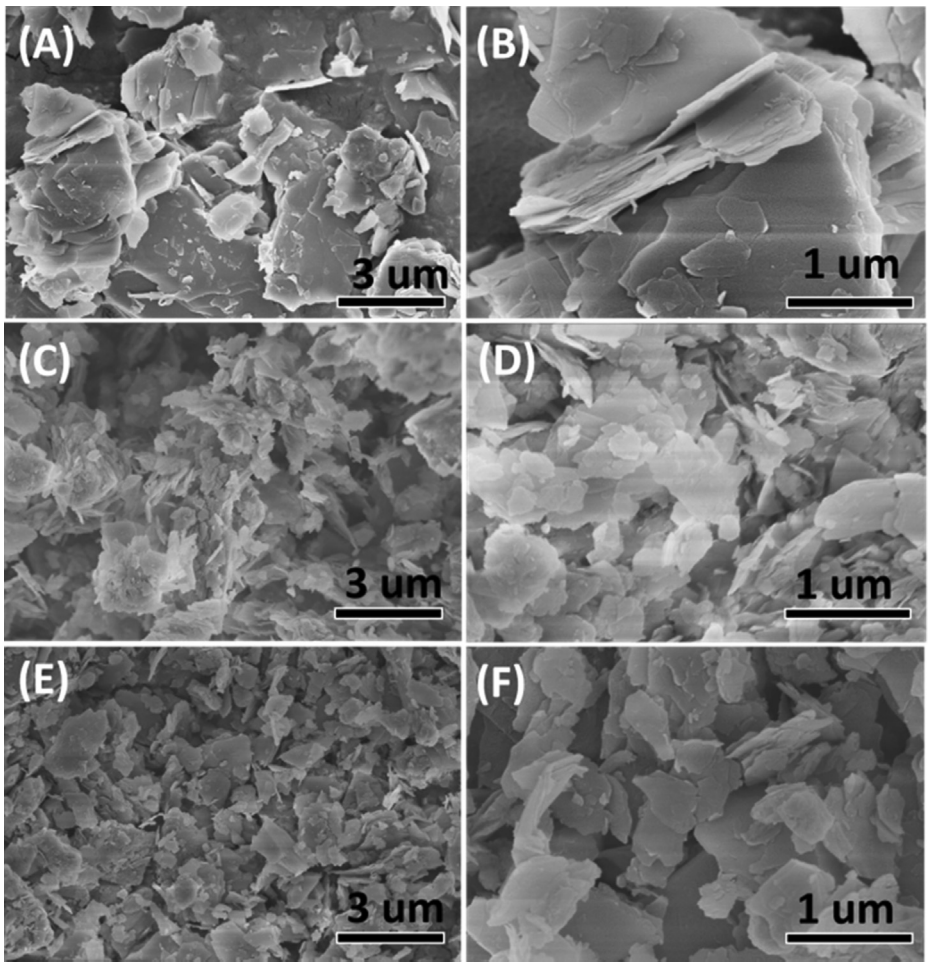

Fig. 2 (A) and (B) SEM images of the original PY powders, (C) and (D) the ball-milled PY without NDZ-201, (E) and (F) the ball-milled MPY with the NDZ-201 addition amount of 0.4 wt%.

Table 1 The N_2 physisorption data of the ball-milled PY samples under various addition amount of NDZ-201.

Sample Name	S_{BET} (m^2/g)	Average pore size[a] (nm)	Average particle size (μm)	Pore volume[b] (cm^3/g)	Micropore volume[c] (cm^3/g)
PY	5.98	17.27	**1.00**	0.0228	0.0008
B-PY	20.28	15.34	0.29	0.0584	0.0021
0.2MPY	23.21	15.42	0.26	0.0717	0.0018
0.3MPY	25.04	13.83	0.24	0.0722	0.0017
0.4MPY	26.37	2.46	0.23	0.0097	0.0025
0.5MPY	24.25	2.45	0.25	0.0094	0.0017
0.8MPY	20.87	2.43	0.29	0.0074	0.0019

[a] , [b] bcalculated from the desorption isotherms by BJH model. [c] calculated by t-plot method. The sample B-PY was the ball-milled PY without coupling agent.

3.2. Hydrophobic property of the MPY

In order to confirm the surface modification of the PY powders, the hydrophobic properties of different samples were analyzed by the measurement of water contact angles. As shown in Fig. 3, the water contact angle of the PY sheet was 46.2°. With the addition of NDZ-201, the water contact angles of the xMPY sheets became larger, confirming the improved hydrophobic properties of these xMPY samples, which can be due to the alkane groups on the modified surface. Besides, the water contact angel of the xMPY sample was increased as the increase of NDZ-201 addition amount when it was less than 0.4 wt%, and the highest contact angle was 120.0° at an addition amount of 0.4 wt% for the 0.4MPY. On the other hand, the water contact angle of the 0.5MPY sheet was decreased after the NDZ-201 beyond 0.4 wt%. With a smaller specific surface area and higher addition amount of NDZ-201 than the 0.4MPY sample, this 0.5MPY sample held lower sur-

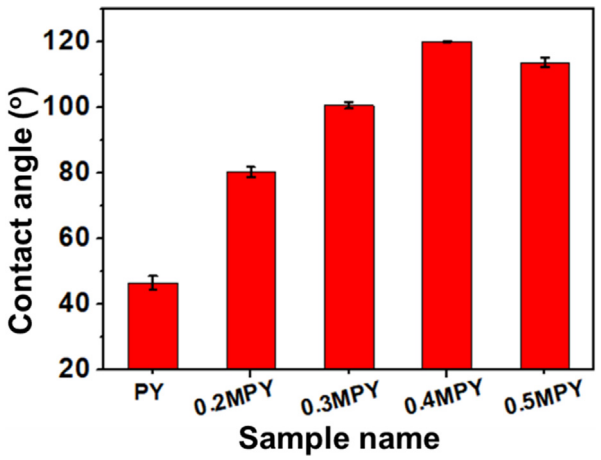

Fig. 3 The water contact angels of the xMPY modified with various addition amount of NDZ-201.

face molar ratio of O/Al (Table S2), indicating less functional groups exposed on the surface that can interact with the NDZ-201 coupling agent, and thus inhibiting the improvement of the hydrophobic property.

3.3. Chemical and structural properties of the MPY/PU

With a filling amount of 5 wt%, the MPY powders were dispersed into the PU matrix, and the properties of the composite coating on the urea granules were studied. As confirmed by the FT-IR spectra of the polymer precursors and the composite materials (Fig. 4 A), the PU polymers were able to physically blend with the PY and MPY fillers. The peak for the stretching vibration of N═C = O (2263 cm^{-1}) was observed in the FT-IR spectrum of toluene diisocyanate (TDI) (Fig. 4 A (a)), while the FT-IR spectrum of the castor oil (CO) presented the characteristics at 3411 cm^{-1} (ν_s, –OH), 2926 cm^{-1} (ν_s, $-CH_2-$), 2855 cm^{-1} (ν_s, $-CH_3$) and 1739 cm^{-1} (ν_s, C═O) (Fig. 4 A (b)). After spraying and curing on urea granules, new peaks at 3434 and 3371 cm^{-1} belong to ν_s (–NH) and ν_{as} (–NH) were occurred in the FT-IR spectrum of the PU polymer and its composite coatings (Fig. 4 A (c-e)), along with the peaks for the ν_s (C—O) and ν_{as} (C—O) at 1222 and 1057 cm^{-1}, respectively. Meanwhile, the peaks assigning to N═C = O groups were almost disappeared in these FT-IR spectra, indicating the formation of PU polymers. In addition, the characteristic peaks for ν_s (Al-OH) at 3674 cm^{-1} and ν_δ (Si-O-Si) at 537 cm^{-1} and 481 cm^{-1} were shown in the FT-IR spectra of the PY/PU and MPY/PU composites (Fig. 4 A (d, e)), suggesting the existence of PY in these composite materials.

In order to avoid the effect of the adsorbed urea on the FT-IR spectra, samples were prepared from the precursor mixtures that were cured in a mold at 65 °C for 24 h, and the filling amounts of PY and 0.4MPY were increased to 20 wt%. Besides, the FT-IR spectra were measured with the crumbs scraped from the upper layers of the prepared films. Similar to the FT-IR spectra of the composite coatings on urea granules, some characteristic peaks relating to the PU polymer and PY were observed (Fig. 4 B). The magnified ones in the range of 4000–3000 cm^{-1} was further shown in Fig. 4 C. Compared to the FT-IR spectra of PY and 0.4MPY, there was almost no shifting for the peak at 3674 cm^{-1} after filling in PY/PU or 0.4MPY/PU films. Besides, the variation for the peak at 3324 cm^{-1} was not obvious for the composite materials while comparing to pure PU, indicating that the possible interactions between the PU and MPY (or PY) was not figured out by the stretching vibration of O—H or N—H. However, some variations were occurred in the region of 1600–1200 cm^{-1} (Fig. 4 D). Compared to the FT-IR spectra of PU and PY/PU, both the peaks at 1533 cm^{-1} and 1385 cm^{-1} shifted slightly to a higher wavenumber for MPY/PU, which meanwhile broaden a little, indicating the possible hydrophobic interactions between the PU and alkyl chains on the surface of MPY. On the other hand, a weak peak appeared around 1240 cm^{-1} for the MPY/PU sample, revealing the stronger interaction of PU with the Si-O of MPY, which may be associated with a H-bonded Si-OH group (Namazi and Mosadegh, 2011; Wang et al., 2006).

In addition, the peak at 3674 cm^{-1} for the MPY/PU-20 % sample was obviously stronger than the PY/PU-20 % (Fig. 4 E). Meanwhile, the FT-IR spectrum for the crumbs from the bottom layer of the PY/PU-20 % was presented in Fig. 4 F, the peak at 3674 cm^{-1} was clearly stronger than the one from the upper layer. These results indicated that the dispersion stability of the modified PY (MPY) was obviously higher than the un-modified one, and thus the MPY powders were easier to interact with the PU polymer and its precursors. This could lead to an increase in the crosslink density of the composites, resulting in the enhancement of the tensile strengths of the MPY/PU composite films (Park and Cho, 2003). Besides, the NDZ-201 modified PY that had alkyl chains was able to serve as the lubricant, which was favorable to improve the elongation at break (Li et al., 2012; Oshita et al., 2019). However, the peak at 2272 cm^{-1} belonging to the stretching vibration of N═C = O was gradually strengthened for the MPY/PU composites while increasing the filling amount from 7 wt% to 20 wt% (Fig. 4 E), which indicated that excessive filling of the MPY would decrease the polyurethane crosslinking density and decline the mechanical properties of the composite films. Therefore, the MPY/PU composite coating with a proper filling amount of MPY was more capable to resist the pressure damage and improve the release longevity of coated fertilizer.

Accordingly, the surface morphology of the PY/PU and MPY/PU membranes was further observed by the SEM images. As revealed by Fig. 5 A, some protrusions with a diameter larger than 2 μm were presented on the surface of the PY/PU membrane, causing the formation of wrinkles around these protrusions. Considering the smaller water contact angle of the PY powders without modification, this phenomenon can be due to the poor compatibility of the PY particles with the PU matrix, which cuased uneven dispersion of the PY powders in the PU matrix. While filling the modified PY powders (MPY) into the PU matrix, the size of the protrusions and wrinkles were clearly reduced on the surface of the MPY/PU membranes (Fig. 5 B-F). Besides, the surface of the MPY/PU membranes become smoother as the increase of NDZ-201 amount, and the one with 0.4 wt% NDZ-201 presented the smoothest surface (Fig. 5 E). This trend was corresponding to the variation of the water contact angles of the xMPY samples, further confirming the effect of their hydrophobic properties on the textural structures of the composite materials.

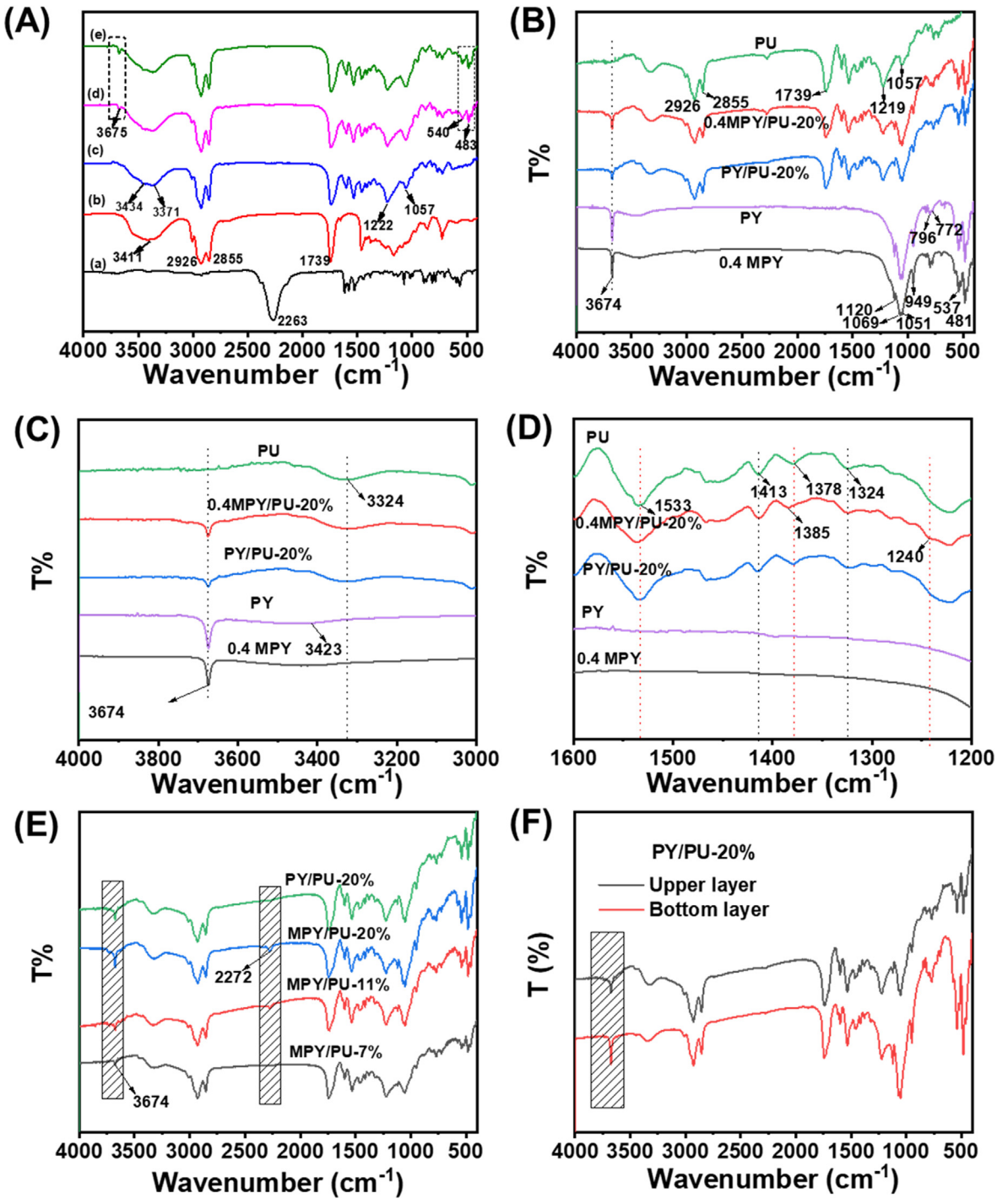

Fig. 4 (A) FT-IR spectra of TDI (a), castor oil (b), and the composite coatings on the urea granules: (c) PU, (d) PY/PU and (e) 0.4MPY/PU that related to a filling percentage of 5 wt%. (B) FT-IR spectra of the PU, PY, 0.4MPY and the PY/PU and 0.4MPY/PU composite films filling with 20 wt% PY or 0.4MPY, and their magnified FT-IR spectra in different ranges: (C) 4000–3000 cm^{-1}, (D) 1600–1200 cm^{-1}. (E) The FT-IR spectra of the upper layers for the composite films of different samples. (F) FT-IR spectra of the PY/PU composite films with a filling amount of 20 wt%.

3.4. Hydrophobic property of the MPY/PU material

Furthermore, the hydrophobic properties of the PU, PY/PU and MPY/PU composite materials were studied by their water contact angles and water absorbencies. It was figured out that the water contact angel (84.2°) of the PY/PU was larger than the pure PU sample (79.3°) (Fig. 6 A). After filling the MPY powders into the PU matrix, the water contact angles of the xMPY/PU composites were first increased and then decreased with the increase of NDZ-201 addition amount (Fig. 6 A), which was similar to the variation of the water contact angles

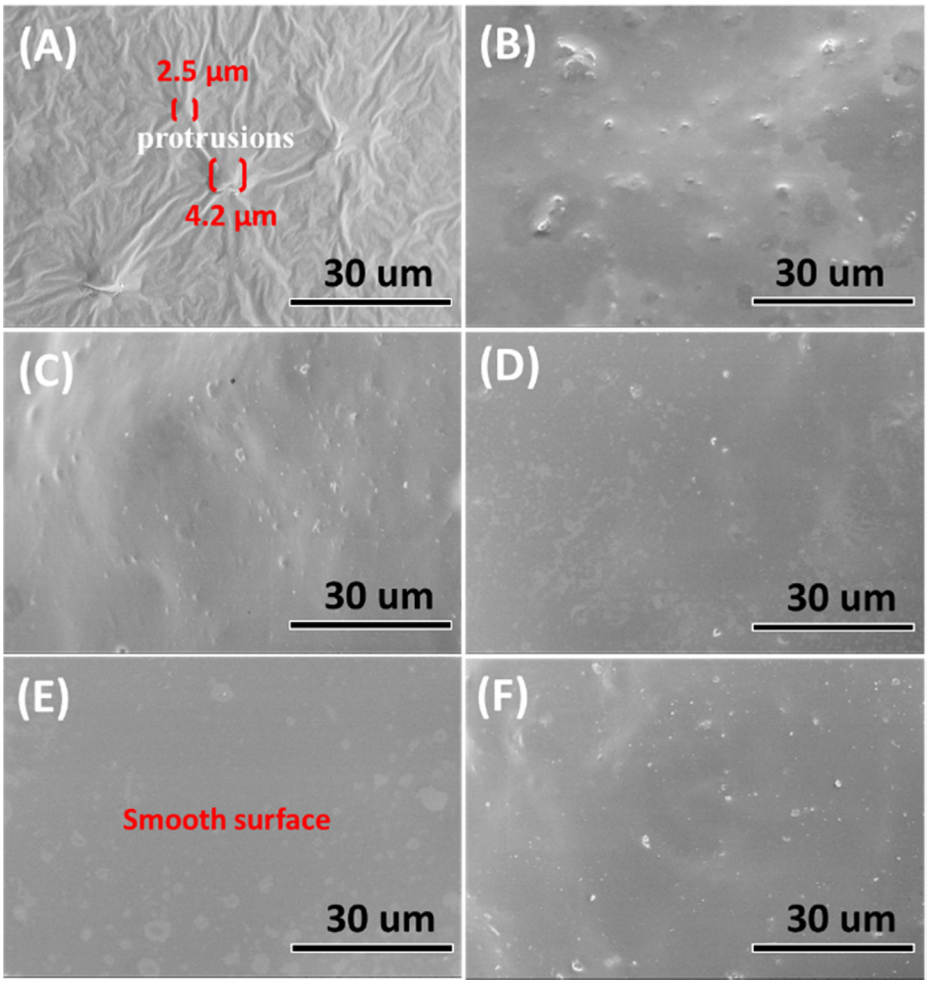

Fig. 5 SEM images of the membranes made of the PU polymers that were filled with MPY modified with various amount of NDZ-201: (A) PY/PU, (B) 0.1MPY/PU, (C) 0.2MPY/PU, (D) 0.3MPY/PU, (E) 0.4MPY/PU and (F) 0.5MPY/PU.

for the xMPY samples (Fig. 3). As discussed above, the alkane groups were modified on the surface of the MPY particles, which can promote the dispersion of the inorganic particles into the PU precursors, and improve the compatibility and pseudo-crosslinking effect of the MPY particles with the PU matrix (Li et al., 2018). However, this effect became weaker for the sample 0.5MPY/PU when the PY particles were treated by 0.5 wt% NDZ-201. This was because that some hydrophilic groups on the surface of the MPY caused poorer dispersion of the MPY particles in PU matrix. Correspondingly, the water absorbency of these composite materials was changed reversely to their water contact angles as proven by Figure S4.

3.5. Mechanical property of the MPY/PU material

Accordingly, the mechanical properties of these MPY/PU composite materials were analyzed by the uniaxial tensible testing at room temperature. Fig. 6 B showed that the tensile strength and elongation at break for the PY/PU composite was slightly smaller compared to the pure PU material. As mentioned above, it can be attributed to the poor compatibility of the PY powders with the PU matrix, and stress sites could be formed around the agglomerates. Specially, these properties were improved while filling the xMPY particles into the PU matrix (Fig. 6 B, xMPY/PU, x = 0.3, 0.4, 0.5). In addition, both the tensile strength and elongation at break were first increased and then decreased as the increased amount of NDZ-201 in the MPY powders, and the highest values were presented by sample 0.4MPY/PU. Compared to the pure PU material, these values were respectively increased by 0.61 MPa and 42 %, which can be due to the improved compatibility of 0.4MPY in the PU matrix and enhanced crosslinking density in this composite material. While increasing the NDZ-201 amount to 0.5 wt%, the agglomerates were observed in the MPY/PU composite material due to the reduced hydrophobic property of the 0.5MPY (Fig. 5 F), resulting in the declining of the mechanical properties.

3.6. Hydrolytic stability of the MPY/PU

While employing the composites as the coating materials of CRF, their resistance to hydrolysis in humid environment is another important factor influencing the controlled-release property, and thus the hydrolytic stability of the PU, PY/PU and 0.4MPY/PU were analyzed by measuring their tensile strengths after immersing in water at 60 °C for 7 days. As shown in Fig. 6 C and D, the tensile strengths of these samples and their elongations at break were all declined to some extent

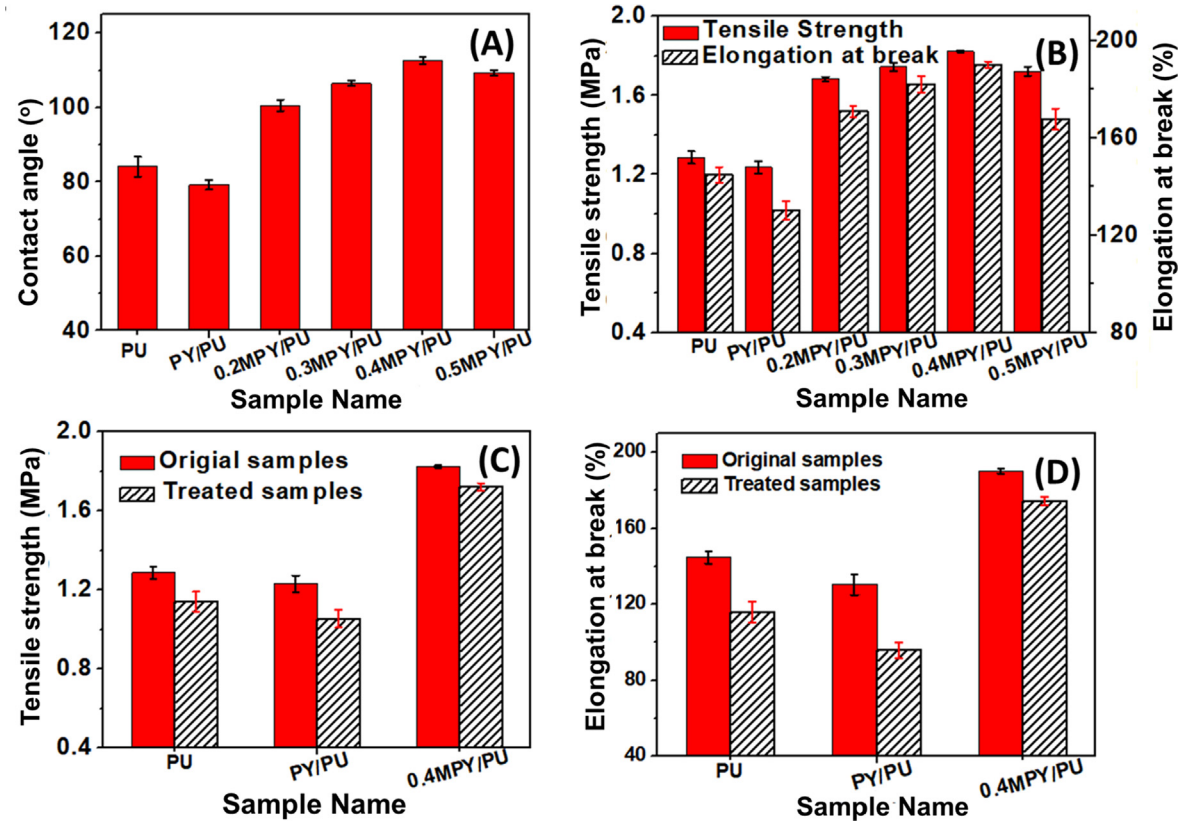

Fig. 6 (A) The water contact angles of PU and its composite materials of PY/PU and xMPY/PU. (B) The tensile strengths and elongations at break for the materials of PU, PY/PU and xMPY/PU that were measured at room temperature. (C) The tensile strengths and (D) elongations at break for the original PU, PY/PU and 0.4MPY/PU, along with the related ones measured after immersing in water at 60 °C for 7 days.

while comparing to the ones before water-immersing, which can be originated from the decreased crosslinking structures by the hydrolysis. The retention of the elongation at break and tensile strength were presented in Table S3, which revealed that the 0.4MPY/PU sample held the highest retention of these properties while the PY/PU had the lowest retention values. This optimized hydrolytic stability of the MPY/PU was possibly due to the improved hydrophobic property and water-swelling resistance, and thus the water molecules were harder to enter the networks of the PU matrix.

3.7. Effect of the MPY filling amount on the properties of the MPY/PU

As discussed above, the PU matrix blending with the MPY treated by 0.4 wt% NDZ-201 performed the best comprehensive properties, and thus the effect of the filling amount on the properties of MPY/PU were further studied based on the 0.4MPY powders. The SEM images (Figure S5 a1-c2) showed that the surface of the MPY/PU membranes were relatively smooth when the filling amount was less than 9 wt%. However, it turned out to be rough when the filling amount was increased to 9 wt% and 11 wt% (Figure S5 d1-e2), meanwhile, protrusions were clearly observed on the surface of the related membranes. Accordingly, when the filling amount was less than 9 wt%, Figure S6 and Figure S7 confirmed that the mechanical properties (tensile strength and elongation at break) and water swelling resistance of the MPY/PU composites were increased as the increase of the MPY filling amount. This was possibly due to the improved pseudo-crosslinking density in the composite materials. On the other hand, these properties for the sample 0.4MYP/PU-7 and 0.4MYP/PU-11 were declined because of the formation of agglomerates in the PU matrix and the reduction of crosslinking structures (Figure S5 d1-e2).

3.8. Controlled-release behaviors of the CRF granules

The nitrogen cumulative release curves of the polyurethane coated urea (PCU) fertilizer, the PY/PCU and xMPY/PCU with the xMPY filling amount of 5 wt% were shown in Fig. 7 A. It was figured out that the nitrogen in the PY/PCU was released by a relatively faster rate than the PCU, and the curve was changed from "S" to an "inverted L" shape. As mentioned above, the PY/PU for the coating material of the PY/PCU fertilizer held a higher water absorbency and poorer mechanical property, resulting in larger cracks during release process as shown in the SEM images (Fig. 8 C), and thus the free water exchange and the release of urea were easier (Liang and Liu, 2006). Reversely, with lower water absorbency and better mechanical properties, the 0.2MPY/PCU, 0.3MPY/PCU and 0.4MPY/PCU performed gradually optimized controlled-release properties (Fig. 7 A). Moreover, the sample 0.4MPY/PCU had the best performance, which respectively

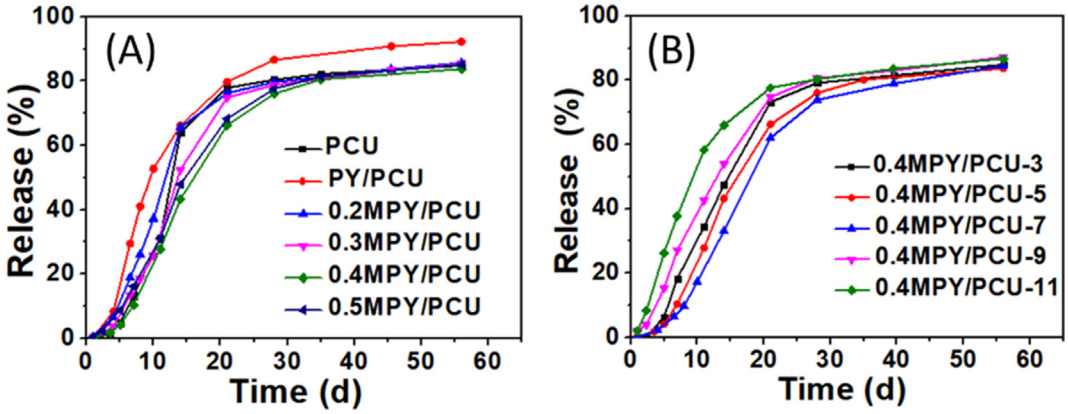

Fig. 7 (A) The curves of nitrogen cumulative release for PCU, PY/PCU, and the xMPY/PCU, corresponding to the MPY with various addition amount of NDZ-201 coupling agent. (B)The curves of nitrogen cumulative release for 0.4MPY/PCU-y, corresponding to the MPY/PU with different filling amounts of the MPY.

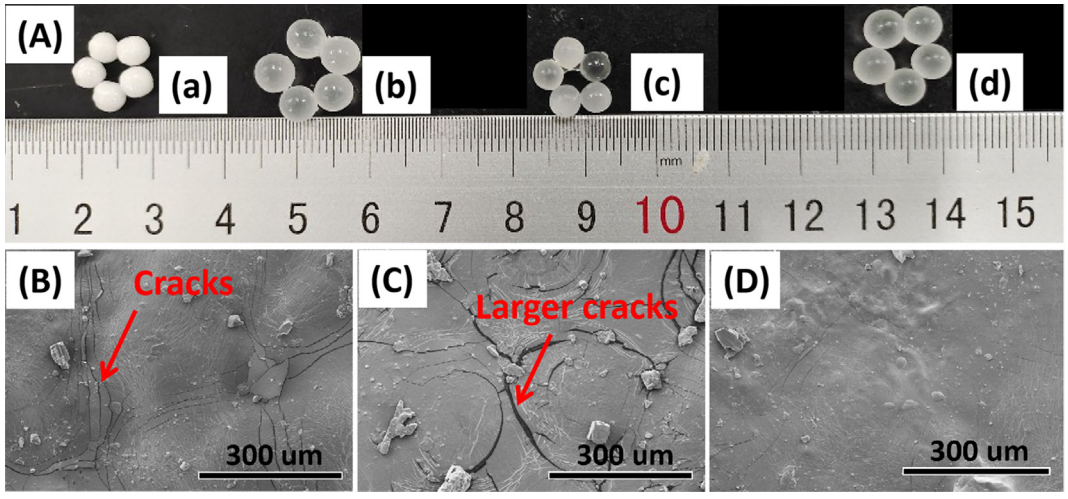

Fig. 8 (A) Photos of the original PCU (a), and the ones immersed in water at 25 °C for 7 days: (b) PCU, (c) PY/PCU-5 and (d) 0.4MPY/PCU-5. The SEM images of the coating surfaces that were observed after freeze-drying the immersed samples: (B) PCU, (C) PY/PCU and (D) 0.4MPY/PCU.

released 1.7 %, 10.4 %, 43.2 %, 66.2 % and 76.1 % of N at 3.5th d, 7th d, 14th d, 21th d and 28th d (Table S4). Accordingly, few cracks were observed in the SEM images of 0.4MPY/PCU after immersing in water at 25 °C for 7 days (Fig. 8 D). These results indicated that the controlled-release properties of the coated CRF can be optimized by the variation of the NDZ-201 coupling amount.

In addition, the controlled-release behaviors can be also tuned by the variation of filling amount of MPY. As shown in Fig. 7 B and Table S5, the nitrogen release rates of the CRF granules were decreased by improving the filling amount of 0.4MPY when it was less than 7 wt% (Table S5), and the sample 0.4MPY/PCU-7 presented the lowest N release of 33.1 %, 62.0 %, 73.9 % and 78.9 % at 14th d, 21th d, 28th d and 40th, respectively. With the optimized controlled release feature and clearly longer release longevity, this CRF should be more effective to meet the requirement of nitrogen for some plant growth than the PU-coated CRF (Mayra E. Gavito et al., 2001; Woli et al., 2017). Accordingly, the duration of 75 % nitrogen release was about 31 days, which was comparable to the recently reported biomass-based PU coatings (Table S6), including the halloysite-modified PU (75 %, 30–38 d) (Wang et al., 2022) and the wheat straw-derived PU (75 %, 32 d) (Yu et al., 2022). While the filling amount beyond 7 wt%, the sample 0.4MPY/PCU-9 and 0.4MPY/PCU-11 released nitrogen in a relatively faster rate (Table S5). This variation was well corresponding to the mechanical properties and water-swelling resistance of the related coating materials (Figure S6 and Figure S7), further confirming the effect of these properties on the controlled-release performance of the CRF fertilizers. As confirmed by the SEM images (Figure S5 d1-e2), agglomerates occurred in the coatings of 0.4MPY/PU-9 and 0.4MPY/PU-11, and the mechanical properties and water swelling resistance were reduced for the related composites (Figure S6 and Figure S7). These factors would result in the formation of apertures in the coating during application, promoting the free water exchange between the solution and the coating networks, and thus increasing the urea release from

the cores. Therefore, an excessive filling amount was disadvantageous to the improve the controlled-release performance of the CRF fertilizers.

4. Conclusions

In summary, the surface of the PY powders were mechanochemically modified with few amounts of NDZ-201 coupling agent, and the modified PY (MPY) particles were filled into the caster-oil based polyurethane matrix. As a result, the comprehensive properties of the MPY/PU composites can be adjusted by controlling the addition amount of NDZ-201 and the filling amount of the MPY powders. By the investigations of the chemical and structural properties of the MPY and the related MPY/PU composites, it was confirmed that the alkoxy groups from the NDZ-201 were reacted with the Al-OH groups on the surface of the PY powders under the mechanochemical treatment, which can improve the hydrophobic properties of the MPY when the addition amount of NDZ-201 was less than 0.5 wt%. After filling these MPY particles into the PU matrix with a proper amount, the dispersibility of the PY particles and their compatibility with PU matrix were optimized, which promoted the pseudo-crosslinking effect of the PY particles, and thus improved the mechanical properties of the MPY/PU composites and their resistance to water-swelling. Synergistically, the controlled-release performance of the CRF with the coating of MPY/PU composites were obviously optimized.

Declaration of Competing Interest

The authors declare that they have no known competing financial interests or personal relationships that could have appeared to influence the work reported in this paper.

Acknowledgements

This work was supported by the Provincial Natural Science Foundation of Fujian, China (Grant No. 2022 J05131, 2021 J01197); and the National Natural Science Foundation of China (Grant No. 22208055, 21825801, 22038002, 83418069, 22178057).

Appendix A. Supplementary material

Supplementary data to this article can be found online at https://doi.org/10.1016/j.arabjc.2022.104400.

References

Ali, M.A., Ahmed, H.A.M., Ahmed, H.M., Hefni, M., 2021. Pyrophyllite: An economic mineral for different industrial applications. Appl. Sci. 11 (23), 11357.

Alisani, R., Rakhshani, N., Abolhallaj, M., Motevalli, F., Abadi, P.G., Akrami, M., Shahrousvand, M., Jazi, F.S., Irani, M., 2022. Adsorption, and controlled release of doxorubicin from cellulose acetate/polyurethane/multi-walled carbon nanotubes composite nanofibers. Nanotechnology 33, (15) 155102.

Amaral, I.F., Granja, P.L., Barbosa, M.A., 2012. Chemical modification of chitosan by phosphorylation: an XPS, FT-IR and SEM study. J. Biomater. Sci. Polym. Ed. 16 (12), 1575–1593.

Azeem, B., KuShaari, K., Man, Z.B., Basit, A., Thanh, T.H., 2014. Review on materials & methods to produce controlled release coated urea fertilizer. J. Control. Release 181, 11–21.

Beig, B., Niazi, M.B.K., Jahan, Z., Hussain, A., Zia, M.H., Mehran, M.T., 2020. Coating materials for slow release of nitrogen from urea fertilizer: a review. J. Plant Nutr. 43 (10), 1510–1533.

Boonchom, B., Baitahe, R., 2009. Synthesis and characterization of nanocrystalline manganese pyrophosphate $Mn_2P_2O_7$. Mater. Lett. 63 (26), 2218–2220.

Bortoletto-Santos, R., Cavigelli, M.A., Montes, S.E., Schomberg, H. H., Le, A., Thompson, A.I., Kramer, M., Polito, W.L., Ribeiro, C., 2020. Oil-based polyurethane-coated urea reduces nitrous oxide emissions in a corn field in a Maryland loamy sand soil. J. Clean. Prod. 249, 119329.

Canada, 2014. Trinity Resources-pyrophyllite pigments/fillers. Foc. Pigments (7), 3-4.

Chen, J., Duan, M., Chen, G., 2012. Continuous mechanical exfoliation of graphene sheets via three-roll mill. J. Mater. Chem. 22 (37), 19625–19628.

Chen, X., Li, Z., Zhang, L., Wang, H., Qiu, C., Fan, X., Sun, S., 2021. Preparation of a novel lignin-based film with high solid content and its physicochemical characteristics. Ind. Crops. Prod. 164, 113396.

Crews, T.E., Peoples, M.B., 2004. Legume versus fertilizer sources of nitrogen: ecological tradeoffs and human needs. Agr. Ecosyst. Environ. 102 (3), 279–297.

Das, S.K., Ghosh, G.K., 2022. Hydrogel-biochar composite for agricultural applications and controlled release fertilizer: A step towards pollution free environment. Energy 242, 122977.

Dubey, A., Mailapalli, D.R., 2019. Zeolite coated urea fertilizer using different binders: Fabrication, material properties and nitrogen release studies. Environ. Technol. Innov. 16, 100452.

Eghbali Babadi, F., Yunus, R., Abdul Rashid, S., Mohd Salleh, M.A., Ali, S., 2015. New coating formulation for the slow release of urea using a mixture of gypsum and dolomitic limestone. Particuology 23, 62–67.

Eghbali Babadi, F., Yunus, R., Masoudi Soltani, S., Shotipruk, A., 2021. Release Mechanisms and kinetic models of gypsum-sulfur-zeolite-coated urea sealed with microcrystalline wax for regulated dissolution. ACS Omega 6 (17), 11144–11154.

Emami, N., Razmjou, A., Noorisafa, F., Korayem, A.H., Zarrabi, A., Ji, C., 2017. Fabrication of smart magnetic nanocomposite asymmetric membrane capsules for the controlled release of nitrate. Environ. Nanotechnol. Monit. Manag. 8, 233–243.

Erdemoğlu, M., Erdemoğlu, S., Sayılkan, F., Akarsu, M., Şener, Ş., Sayılkan, H., 2004. Organo-functional modified pyrophyllite: preparation, characterisation and Pb(II) ion adsorption property. Appl. Clay Sci. 27 (1–2), 41–52.

Fertahi, S., Ilsouk, M., Zeroual, Y., Oukarroum, A., Barakat, A., 2021. Recent trends in organic coating based on biopolymers and biomass for controlled and slow release fertilizers. J. Control. Release 330, 341–361.

Fukushima, Y., Tada, I., Nanao, H., Mori, S., Aoki, S., 2016. Combined effect of phosphate ester and OBCS on tribochemical decomposition of hydrocarbon oil on nascent steel surfaces. Tribol. Lett. 63 (1), 1–8.

Gavito, M.E., Curtis, P.S., Mikkelsen, T.N., Jakobsen, I., 2001. Interactive effects of soil temperature, atmospheric carbon dioxide and soil N on root development, biomass and nutrient uptake of winter wheat during vegetative growth. J. Exp. Bot. 52 (362), 1913–1923.

Haitao, L., Jingfeng, Z., Shie, L., Xuejun, W., Weidong, X., 2012. Study on the effect of properties of SBR/N330 nanocomposites filled with different shape pyrophyllite composite powders. Rare Metal Mat. Eng. 41, 137–139.

Harvey, C., Murray, H., 1997. Industrial clays in the 21st century: A perspective of exploration, technology and utilization. Appl. Clay Sci. 11, 285–310.

Haseeb ur, R., Asghar, M.G., Ikram, R.M., Hashim, S., Hussain, S., Irfan, M., Mubeen, K., Ali, M., Alam, M., Ali, M., Haider, I., Shakir, M., Skalicky, M., Alharbi, S.A. and Alfarraj, S., 2022. Sulphur coated urea improves morphological and yield characteristics of transplanted rice (Oryza sativa L.) through enhanced nitrogen uptake. J. King Saud Univ. Sci. 34(1), 101664.

Hu, Z.-Y., Chen, G., Yi, S.-H., Wang, Y., Liu, Q., Wang, R., 2021. Multifunctional porous hydrogel with nutrient controlled-release and excellent biodegradation. J. Environ. Chem. Eng. 9, (5) 106146.

Hu, H., Wang, X., Lee, K.I., Ma, K., Hu, H., Xin, J.H., 2016. Graphene oxide-enhanced sol-gel transition sensitivity and drug release performance of an amphiphilic copolymer-based nanocomposite. Sci. Rep. 6, 31815.

Kenawy, E.-R., Azaam, M.M., El-nshar, E.M., 2019. Sodium alginate-g-poly(acrylic acid-co-2-hydroxyethyl methacrylate)/montmorillonite superabsorbent composite: Preparation, swelling investigation and its application as a slow-release fertilizer. Arab. J. Chem. 12 (6), 847–856.

Kiran, Tiwari, R., Krishnamoorthi, S. and Kumar, K., 2019. Synthesis of cross-linker devoid novel hydrogels: Swelling behaviour and controlled urea release studies. J. Environ. Chem. Eng. 7(4), 103162.

Lawrencia, D., Wong, S.K., Low, D.Y.S., Goh, B.H., Goh, J.K., Ruktanonchai, U.R., Soottitantawat, A., Lee, L.H., Tang, S.Y., 2021. Controlled release fertilizers: A review on coating materials and mechanism of release. Plants 10 (2), 238.

Li, L., Sun, Y., Cao, B., Song, H., Xiao, Q., Yi, W., 2016. Preparation and performance of polyurethane/mesoporous silica composites for coated urea. Mater. Des. 99, 21–25.

Li, L., Cao, B., Sun, Y., Yi, W., Ni, X., Xiao, Q., 2018. Effect of filler treatment on the release properties of coating on urea granules. Polym.-Plast. Tech. Mat. 58 (1), 77–82.

Li, Q., Wu, S., Ru, T., Wang, L., Xing, G., Wang, J., 2012. Synthesis and performance of polyurethane coated urea as slow/controlled release fertilizer. Journal of Wuhan University of Technology-Mater. Sci. Ed. 27 (1), 126–129.

Liang, R., Liu, M., 2006. Preparation and properties of a double-coated slow-release and water-retention urea fertilizer. J. Agr. Food Chem. 54 (4), 1392–1398.

Lin, K., Zhao, Y.-P., 2019. Mechanical peeling of van der Waals heterostructures: Theory and simulations. Extreme Mech. Lett. 30, 100501.

Liu, X., Chen, F., Yang, H., Xu, W., 2013. Feasibility and properties of polypropylene composites reinforced with down feather whisker. J. Thermoplast. Compos. Mater. 28 (1), 19–31.

Liu, J., Yang, Y., Gao, B., Li, Y.C., Xie, J., 2019. Bio-based elastic polyurethane for controlled-release urea fertilizer: Fabrication, properties, swelling and nitrogen release characteristics. J. Clean. Prod. 209, 528–537.

Lohmousavi, S.M., Abad, H.H.S., Noormohammadi, G., Delkhosh, B., 2020. Synthesis and characterization of a novel controlled release nitrogen-phosphorus fertilizer hybrid nanocomposite based on banana peel cellulose and layered double hydroxides nanosheets. Arab. J. Chem. 13 (9), 6977–6985.

Monash, P., Pugazhenthi, G., 2010. Removal of crystal violet dye from aqueous solution using calcined and uncalcined mixed clay adsorbents. Sep. Sci. Technol. 45 (1), 94–104.

Namazi, H., Mosadegh, M., 2011. Preparation and properties of starch/nanosilicate layer/polycaprolactone composites. J. Polym. Environ. 19 (4), 980–987.

Oshita, K., Komiyama, S., Sasaki, S., 2019. Effects of surface texturing pattern on the lubricity of mica-organic hybrid solid lubricants and parametric evaluation of their cleavabilities. Tribol. Int. 140, 105842.

Parekh, B.B., Joshi, M.J., 2007. Growth and characterization of gel grown calcium pyrophosphate tetrahydrate crystals. Cryst. Res. Technol. 42 (2), 127–132.

Park, S.-J., Cho, K.-S., 2003. Filler-elastomer interactions: influence of silane coupling agent on crosslink density and thermal stability of silica/rubber composites. J. Colloid Interface Sci. 267 (1), 86–91.

Pereira, E.I., Giroto, A.S., Bortolin, A., Yamamoto, C.F., Marconcini, J.M., de Campos Bernardi, A.C. and Ribeiro, C., 2015. Perspectives in nanocomposites for the slow and controlled release of agrochemicals: Fertilizers and Pesticides. Chapter 11, 241-265.

Pradhan, A., Das, M., Goswami, S., 2015. Economic Potential of Pyrophyllite Deposits of Keonjhar as Industrial Mineral. Vistas Geol. Res., 86–90

Qin, X., Zhao, J., Wang, J., He, M., 2020. Atomic structure, electronic, and mechanical properties of pyrophyllite under pressure: A first-principles study. Minerals 10, 778.

Ristić, I.S., Bjelović, Z.D., Holló, B., Mészáros Szécsényi, K., Budinski-Simendić, J., Lazić, N., Kićanović, M., 2012. Thermal stability of polyurethane materials based on castor oil as polyol component. J. Therm. Anal. Calorim. 111 (2), 1083–1091.

Salimi, M., Motamedi, E., Motesharezedeh, B., Hosseini, H.M., Alikhani, H.A., 2020. Starch-g-poly(acrylic acid-co-acrylamide) composites reinforced with natural char nanoparticles toward environmentally benign slow-release urea fertilizers. J. Environ. Chem. Eng. 8, (3) 103765.

Sempeho, S.I., Kim, H.T., Mubofu, E., Hilonga, A., 2014. Meticulous overview on the controlled release fertilizers. Advances in Chemistry, 1–16.

Snyder, G.H. and Gasch, G.J., 1976. Sulfur-coated fertilizers for sugarcane: II. Release characteristics of sulfur-coated urea and KCl1, Soil. Sci. Soc. Am. J. 40 (1) (1976) 122-126.

Song, J., Ke, R., Zhang, M., Fei, G., Ma, X., Qiu, J., 2019. Interface interaction and compatibility molecular dynamics verification of Scutellaria baicalensis Georgi extracts/PBS dyeing and antibacterial composites. Mater. Res. Express. 6, (7) 075403.

Souza, I.M.S., Gurgel, G.C.S., Medeiros, A.M., Zonta, E., Ruiz, J.A. C., Paskocimas, C.A., Motta, F.V., Bomio, M.R.D., 2018. The use of clinoptilolite as carrier of nitrogened fertilizer with controlled release. J. Environ. Chem. Eng. 6 (4), 4171–4177.

Temuujin, J., Okada, K., Jadambaa, T.S., MacKenzie, K.J.D., Amarsanaa, J., 2003. Effect of grinding on the leaching behaviour of pyrophyllite. J. Eur. Ceram. Soc. 23, 1277–1282.

Tian, H., Liu, Z., Zhang, M., Guo, Y., Zheng, L., Li, Y.C., 2019. Biobased polyurethane, epoxy resin, and polyolefin wax composite coating for controlled-release fertilizer. ACS Appl. Mater. Interfaces 11 (5), 5380–5392.

Vejan, P., Khadiran, T., Abdullah, R., Ahmad, N., 2021. Controlled release fertilizer: A review on developments, applications and potential in agriculture. J. Control. Release 339, 321–334.

Wang, Q., Dong, F., Dai, J., Zhang, Q., Jiang, M., Xiong, Y., 2019. Recycled-oil-based polyurethane modified with organic silicone for controllable release of coated fertilizer. Polymers 11 (3), 454–469.

Wang, X., Du, Y., Yang, J., Wang, X., Shi, X., Hu, Y., 2006. Preparation, characterization and antimicrobial activity of chitosan/layered silicate nanocomposites. Polymer 47 (19), 6738–6744.

Wang, X., Hu, H., Wang, W., Lee, K.I., Gao, C., He, L., Wang, Y., Lai, C., Fei, B., Xin, J.H., 2016. Antibacterial modification of an injectable, biodegradable, non-cytotoxic block copolymer-based physical gel with body temperature-stimulated sol-gel transition and controlled drug release. Colloids Surf. B 143, 342–351.

Wang, C., Song, S., Yang, Z., Liu, Y., He, Z., Zhou, C., Du, L., Sun, D., Li, P., 2022. Hydrophobic modification of castor oil-based polyurethane coated fertilizer to improve the controlled release of nutrient with polysiloxane and halloysite. Prog. Org. Coat. 165, 106756.

Woli, K.P., Sawyer, J.E., Boyer, M.J., Abendroth, L.J., Elmore, R.W., 2017. Corn era hybrid dry matter and macronutrient accumulation across development stages. Agron. J. 109 (3), 751–761.

Yang, Y.C., Zhang, M., Li, Y., Fan, X.H., Geng, Y.Q., 2012. Improving the quality of polymer-coated urea with recycled plastic, proper additives, and large tablets. J. Agric. Food Chem. 60 (45), 11229–11237.

Yeganeh, H., Mehdizadeh, M.R., 2004. Synthesis and properties of isocyanate curable millable polyurethane elastomers based on castor oil as a renewable resource polyol. Eur. Polym. J. 40 (6), 1233–1238.

Yu, X., Zhong, H., Liu, G., 2010. Reverse flotation of diaspore from aluminosilicates by a new cationic organosilicon quaternary ammonium collector. Mater. Metall. Process. 27 (3), 173–178.

Yu, X., Sun, X., Dong, J., Wu, L., Guo, W., Wang, Y., Jiang, X., Liu, Z., Zhang, M., 2022. Instant catapult steam explosion pretreatment of wheat straw liquefied polyols to prolong the slow-release longevity of bio-based polyurethane-coated fertilizers. Chem. Eng. J. 435, 134985.

Zhao, S.M., Wang, D.Z., Hu, Y.H., Liu, B.D., Xu, J., 2003. The flotation behaviour of N-(3-aminopropyl)-dodecanamide on three aluminosilicates. Miner. Eng. 16 (12), 1391–1395.

Zheng, W., Zhang, M., Liu, Z., Zhou, H., Lu, H., Zhang, W., Yang, Y., Li, C., Chen, B., 2016. Combining controlled-release urea and normal urea to improve the nitrogen use efficiency and yield under wheat-maize double cropping system. Field Crops Res. 197, 52–62.